Ocean heat content and its role in tropical cyclogenesis for the Bay of Bengal basin

Jiya Albert[1] · Prasad K. Bhaskaran[1]

Abstract

Anthropogenic factors continue to warm the oceans by storing sufficient memory of past accumulated effects resulting in higher Sea surface temperature (SST) and Ocean heat content (OHC) invigorating tropical cyclogenesis and tropical cyclone intensity. Prior studies indicate that an increase in accumulated tropical cyclone heat potential, a measure of OHC is directly related to high intense storms of longer durations. The present study is an attempt to understand the role of OHC in tropical cyclogenesis for the Bay of Bengal (BoB). Unlike the other global ocean basins, the BoB is a semi-marginal sea in the North Indian Ocean (NIO) having differential water mass characteristics attributed due to tremendous influx from riverine discharges, seasonal reversing monsoonal wind system and complex ocean circulation features. This study provides a detailed assessment on SST and OHC distributions during the pre- and post-monsoon seasons covering a period of 21 years (1991–2016) over four identified sub-domains, the potential locations for tropical cyclogenesis. The daily ERA-Interim, ORAS4, ORAS5 and 3-h RAMA buoy datasets were used in the present study. The spatial distribution and variations of SST and OHC anomalies during pre- and post-monsoon seasons in the BoB were also examined. Differential nature of inter-annual SST variability was noticed in the study region. Highest variability in SST is evidenced during both pre- and post-monsoon seasons for the northern Bay region showing a warming bias of ~ 1.7 °C in the past 2 decades. Contrasting variability is also noticed for the eastern Bay during pre-monsoon that is almost three times higher as compared to the post-monsoon season. Maximum OHC variability is found for the southern and central-eastern Bay regions. It is seen that OHC variability has a strong tele-connection with Oceanic Niño Index associated with El Niño/La Niña events in the Pacific basin with their amplitudes found to increase from northern to southern regions of the Bay.

Keywords Ocean heat content · SST · Tropical cyclogenesis · Tele-connections

1 Introduction

Tropical cyclones form over the warm ocean basins and eventually influenced by the action of steering forces that guides its pathway towards the land. The Bay of Bengal (BoB) located in the North Indian Ocean (NIO) is a quite active region for tropical cyclogenesis. The annual occurrence frequency is about five cyclones, having differential characteristics in terms of translational speed and intensification process. The environmental conditions conducive for tropical cyclone formation and the role of oceanic component in particular were investigated in this study. Especially over the NIO basin, tropical cyclone activity is quite unique and that exhibits a bimodal distribution in the annual frequency. The pre- and post-monsoon season covers the period from March to May and from October to December respectively. Peak tropical cyclone activity occurs during the pre- and post-monsoon seasons (Alam et al. 2003; Evan and Camargo 2011; Yanase et al. 2012; Li et al. 2013). Kossin et al. (2014) postulated that cyclogenesis locations experienced a poleward shift in almost all the global ocean basins. However, a study by Sahoo and Bhaskaran (2016) confirms the absence of poleward migration concerning past tropical cyclones that formed in BoB basin. Their study (Sahoo and Bhaskaran 2016) analysed the decadal distribution of cyclogenesis over this basin for the past 4 decades confirming that the active region for cyclogenesis is the central Bay bounded between the geographical coordinates 6°

✉ Prasad K. Bhaskaran
  prasadlsu@yahoo.com; pkbhaskaran@naval.iitkgp.ac.in

1 Department of Ocean Engineering and Naval
   Architecture, Indian Institute of Technology Kharagpur,
   Kharagpur 721 302, India

N–14° N; 85° E–93° E. An in-depth analysis was carried out (Sahoo and Bhaskaran 2016) to investigate the poleward shift hypothesis proposed by Kossin et al. (2014) for this basin. Results from their study (Sahoo and Bhaskaran 2016) indicate that poleward shift on decadal scale is quite unlikely; however, the study highlights on an oscillatory trend in cyclogenesis locations. Also, it mentions that the oscillatory pattern is comparable with shift in SST on decadal time scales, and in the recent decade there is a high probability on possible shift in cyclogenesis location migrating towards the eastern sector (within 93° E−100° E). In addition, to establish a better clarity on shift in cyclogenesis locations, Sahoo and Bhaskaran (2016) divided the entire Bay into four geometrically disconnected regions. Transect along 90° East Ridge was chosen as a reference thereby dividing the entire Bay into east–west and north–south directions. Analysis of the four sub-divided regions having distinct water mass characteristics can provide a better clarity on tropical cyclogenesis formation. Analysis for the south-central BoB (west of the 90° E ridge) showed that decadal variability of cyclogenesis exhibited an oscillatory pattern with a distinct decadal shift along the north–south direction. For regions located in the eastern side of south-central BoB, the decadal variability showed an east–west oscillatory nature.

Magee and Verdon-Kidd (2018) developed a relationship connecting the Indian Ocean SST variability and tropical cyclogenesis characteristics in the southwest Pacific Ocean by statistically relating indices of Indian Ocean SST variability to southwest Pacific tropical cyclogenesis locations. Their study also investigated the physical mechanisms driving the observed relationship by examining changes in the environmental conditions conducive for tropical cyclogenesis. Interestingly, the study demonstrates that SST variability over Indian Ocean significantly modulates the cluster pattern of southwest Pacific tropical cyclogenesis, wherein warmer (cooler) SSTs over eastern and western Indian Ocean region results in a statistically significant north/east (south/west) migration of tropical cyclogenesis by up to 950 km. Mawren and Reason (2016) studied the variability of upper ocean characteristics and its relation to tropical cyclones in the southwest Indian Ocean. Their study for the southwest Indian Ocean showed that upper OHC and barrier layer thickness influence the tropical cyclone intensification process, as well the rapid intensification is influenced by large OHC, thick barrier layers and presence of anti-cyclonic eddies. Over NIO basin during the pre-monsoon season, deficiency of barrier layer along with larger enthalpy flux and presence of large accumulated heat potential (Vissa et al. 2013) can lead tropical cyclone intensification. The importance of large OHC towards tropical cyclone generation in the southwest Indian Ocean has been demonstrated in their study (Mawren and Reason 2016).

The upper OHC and ENSO variability are intrinsically connected with alternating stages of OHC build-up and discharge as reported by few studies for the equatorial Pacific Ocean (Wyrtki 1985; Cane et al. 1986; Zebiak 1989). Another study by Jin (1997) who formulated the Recharge Oscillator theory of ENSO described a relationship between OHC, SST and zonal wind stress and studies conducted later confirmed these relationships highlighting its importance in understanding the ENSO dynamics cycle (Meinen and McPhaden 2000; Trenberth et al. 2002). Another interesting study by Rajeevan and McPhaden (2004) links the equatorial Pacific OHC as a useful predictor for Indian Summer Monsoon (ISM) rainfall. Felton et al. (2013) showed that Niño-3.4 index is negatively correlated with tropical cyclone activity over the BoB with a lead time of about 5 months. Girishkumar and Ravichandran (2012) reported that during La Niña events, the Tropical Cyclone Heat Potential (TCHP) and low-level vorticity over NIO are relatively large as compared to El Niño events and that favours the development of tropical cyclones. In a very recent study, the evolution of OHC pertaining to ENSO was investigated by Cheng et al. (2019). Their study highlighted that ENSO dominates the variability in the ocean energy budget. By combining observational data, reanalysis, surface heat flux from Earth System Model simulations, the redistribution of energy within the Earth System during ENSO events including exchanges between ocean-atmosphere at different ocean basins are reported. Their results (Cheng et al. 2019) confirmed a strong negative OHC tendency in the tropical Pacific Ocean during El Niño events attributed due to enhanced air-sea heat fluxes into atmosphere driven by high SSTs. Also, their study indicated on adiabatic redistribution of heat both laterally and vertically (0–100 m and 100–300 m) in the tropical Pacific and Indian Ocean basins that dominate the local OHC tendency. During La Niña events, the accumulation of heat in the western tropical Pacific is accompanied by higher than normal sea level and also associated with deeper than normal thermocline highlighting the vertical redistribution of heat in the Indo-Pacific Ocean basin (Cheng et al. 2019). Especially during La Niña events, the transport of heat through the Indonesian Through flow influences the heat budget over Pacific and Indian Ocean basins on inter-annual time scales (Sprintall et al. 2009; Mayer et al. 2014, 2018). Also, changes in surface wind due to ENSO phenomena plays an important role in upper ocean circulation dynamics and the local ocean heat transport in both Atlantic and Indian Oceans (Latif and Grötzner 2000; Yeh et al. 2018). It is also noted that warming in the tropical Indianand Atlantic Oceans during El Niño evens largely offsets the Pacific cooling(Cheng et al. 2019). From the above studies, the tele-connection can inducespatial variations over

the BoB region, however the different response of tropical cyclones to these variations is an active area of research that requires a separate detailed study.

The present study is an effort to understand the importance of OHC in the BoB that is quite active in tropical cyclogenesis. A detailed evaluation was carried out to examine the trends in SST and OHC parameters over this basin. Short-term climatological trend (1996–2016) in both SST and OHC fields were investigated in this study utilizing data from various sources such as: ERA-Interim, ORAS4 (Ocean Reanalysis System version 4), ORAS5 (Ocean Reanalysis System version 5), and RAMA (Research Moored Array for African-Asian-Australian Monsoon Analysis and Prediction) buoys during pre- and post-monsoon seasons. Further, a strong correlation was seen in the ONI (Oceanic Niño Index) that considers El Niño and La Niña episodes with OHC distribution over this basin. This paper is organized as follows: Sect. 2 deals with the Study area and aspects related to tropical cyclones in the BoB. Section 3 covers the Data and Methodology and the diagnostic parameters used in the present study. The Results and Discussion are dealt in Sect. 4 covering a critical evaluation on the SST and OHC variability at four sub-domains in the BoB basin. In addition, the tele-connection linkage between ONI in the Pacific Ocean and OHC are also discussed. Finally, the Sect. 5 deals with the overall conclusions obtained from this study.

2 Study domain

The BoB is a semi-marginal sea located in the NIO basin that is quite active in tropical cyclogenesis and a potential region for the intensification of cyclones. Annually this region contributes nearly 7% of the total count of global tropical storms (Gray 1968). Cyclonic disturbances that develop over this region can be grouped as: tropical depression, tropical storms and severe tropical storms classified based on their maximum sustained wind speed as per the India Meteorological Department (IMD). Annual percentage distribution of storms by analysing 100 years of data (Mohanty 1994) indicates that more than 60% of cyclonic disturbances develop during the period July–October, and about 2% occur during the period January–March. Figure 1 illustrates the NIO basin and each representative box marked from 1 to 4 in BoB corresponds to a grid size of 5° × 5° representing the different sub-domains used in the present study for a detailed analysis of SST and OHC parameters. The division for four sub-domains (covering northern, central, eastern and southern bay) are based on the differential water mass characteristics, and also keeping in view these sub-domains are active tropical cyclogenesis location in the BoB basin. Table 1 provide more details on the statistics of cyclonic storms categorized into depression (D),
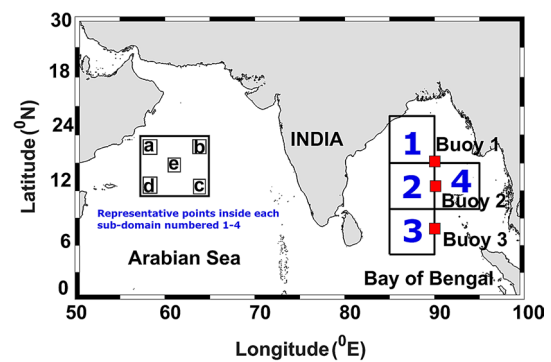

Fig. 1 Study area showing the four sub-domains numbered from 1 to 4 covering northern (1), central and eastern (2 and 4), and southern (3) regions in the Bay of Bengal. Representative points inside each sub-domain for the boxes numbered 1–4 for SST and OHC analysis are marked by letters (a–e). RAMA buoy locations are marked by red boxes

cyclonic storm (CS), and severe cyclonic storm (SCS) that formed over the four sub-domains, including the percentage of events as well the size of each sub-domain. Sahoo and Bhaskaran (2016) provide a detailed assessment and evaluation on the historical cyclone tracks that formed over this basin using the cluster analysis. Their study Sahoo and Bhaskaran (2016) performed a comprehensive analysis on the decadal migration of tropical cyclogenesis utilizing the archived data of past four decades. The four boxes shown in Fig. 1 (numbered from 1 to 4), maps the cyclogenesis locations as reported by Sahoo and Bhaskaran (2016). The respective locations of RAMA buoys, an array of in situ observations moored along the 90° E transect are represented in red solids squares (Fig. 1).

3 Data and methodology

This study considered a total of 98 cyclonic events that includes depression, cyclonic storm, and severe cyclonic storm categories during the period 1996–2016. The IMD E-Atlas reported a total number of 125 events during this time frame that includes the above-mentioned categories. The NIO region shown in Fig. 1 accounted nearly 98 events and that is about 79% of the total count. More details are provided in Table 1. The present study critically evaluated the surface and sub-surface parameters such as SST and OHC during 1996–2016 and examined its role in tropical cyclogenesis. Heat content in the oceanic layer plays a major role in supporting tropical cyclone formation as well its intensification. Maximum energy supplied by the oceans is available in upper 300 m water depth. Therefore, three independent datasets, one for SST and the other two for OHC integrated over the upper 300 m of oceanic layer (D300) were used in this study to carry out a detailed analysis. The NOAA-WOD

Table 1 Details of the four sub-domains and statistics of cyclonic storms corresponding to each sub-domain during the study period

Sub-domains	D	CS	SCS	Latitude/Longitude	% of events occurred
1	21	13	6	15° N−20° N; 85° E−90° E	40.8
2	9	5	0	10° N−15° N; 85° E−90° E	14.3
3	8	4	5	5° N−10° N; 85°E−90° E	17.3
4	16	7	4	10° N−15° N; 90°E−95° E	27.5

D depression, *CS* cyclonic storm, *SCS* severe cyclonic storm

is a quality-controlled product at standard depths developed by blending various sources of in situ observations for the global oceans. The dataset is a global one-degree gridded climatological mean fields of oceanographic variables at standard depths. Popularly, the NOAA-WOD dataset is being widely used as initial and boundary conditions for ocean models and coupled climate models. The ORAS4 and ORAS5 is an assimilated reanalysis product developed using quality-controlled in situ observations of the global oceans at a much higher temporal resolution (daily data) as compared to NOAA-WOD database. As compared to ORAS4, the upgraded ORAS5 product has many advantages in model and data assimilation method, forcing parameters and observational datasets. The ORAS4 has 42 vertical levels, whereas it is 75 in the ORAS5 product. Direct surface fluxes from ERA40 and ERA-Interim are used to generate ORAS4; however, the ERA-Interim with bulk formula and wave forcing is used in ORAS5. Also, the ORAS4 used the multi-scale bias correction and the same with ensemble approach was used in ORAS5. The time frame from 1959 to present is the reanalysis period for ORAS4, whereas it is from 1979 to present with a spin-up from 1958 onwards in the ORAS5 product. In addition, the spatial resolution in the Ocean Reanalysis product is higher as compared to the WOD product. Considering these merits, the ORAS4 and ORAS5 is preferred for analysis in the present study as compared to NOAA-WOD. The data from array of in situ RAMA buoys located along the 90° E meridional transect was also used in the present study. Table 2 provides an overview on the various datasets used in this study. This study was carried out in two parts. Firstly, it focused on understanding the mechanism of cyclone intensification and its correlation with SST datasets during the pre- and post-monsoon seasons (1996–2016) along the four sub-domains in BoB (shown in Fig. 1). Further, the study also investigated the OHC variability at these

sub-domains and the RAMA buoy locations. The study further evaluated the seasonal anomaly distribution of OHC and SST over pre and post monsoon seasons. An anomaly of SST and OHC is the difference between an actual value and its long-term average (1996−2016). The individual month long-term average for SST and OHC data were estimated and represented as SST_m and OHC_m respectively. The difference between the corresponding monthly value and its long-term average ($SST− SST_m$ and $OHC− OHC_m$) is represented as the anomaly plot for the 21 years (1996−2016). The OHC was estimated using the mathematical relation: $H = \rho C_p \int_{h1}^{h2} T(z)dz$, where '$\rho$' is the seawater density; 'C_p' represents the seawater specific heat; and '$T(z)$' represents the temperature as a function of water depth (z) integrated over the column from surface to 300 m water depth.

3.1 ERA-interim data

The ERA-Interim is a global atmospheric reanalysis product generated using an advanced data assimilation procedure by ECMWF (European Centre for Medium Range Weather Forecasts). The data assimilation system is based on the IFS (Cy31r2). More details about this dataset are available in Dee et al. (2011). This dataset used in the present study is superior as compared to ERA-40. The lower boundary condition prescribed in ERA-Interim is from various sources depending on the date of reanalyses. For SST data corresponding to the period January 1989–June 2001, the NCEP 2D-Var SST that utilized in situ data from buoys and ships; before 1998 the COADS (Comprehensive Ocean-Atmosphere Data Set) and after 1998 the Global Telecommunication System (GTS) and AVHRR satellite datasets are being used. For the period July 2001–December 2001, the NOAA Optimum Interpolation SST v2 (NCEP OISST v2) was used. Accordingly, for the period January 2002–January 2009, the

Table 2 Details of datasets used in the present study

Model	ERA-Interim	ORAS4	ORAS5	RAMA Buoys
Temporal resolution	Daily	Daily	Daily	3 h
Spatial resolution/ Location	0.25° × 0.25°	0.25° × 0.25°	0.25° × 0.25°	I—15° N/90° E II—12.5° N /90° E III—8.5° N /90° E

NCEP RTG (Real-time Global SST) was used. Similarly, for the period from February 2009 onwards the Meteorological Office Operational SST and OSTIA were used that combined information from ICOADS in situ data, OSISAF sea ice data, AVHRR satellite and ATSR instruments. This study used the daily SST field having a horizontal grid resolution of 0.25° × 0.25°.

3.2 Ocean Reanalysis System (ORAS4) and (ORAS5) data

The ECMWF implemented ORAS4 (Operational Ocean Reanalysis System) covering the period from 1958 to present. The ORAS4 incorporates the NEMOVAR that used 4D-Var algorithm in producing realistic global analysis. The dataset is an assimilated product using different types of temperature and salinity profiles such as from Expendable Bathythermograph (XBT with only temperature profiles), Conductivity-Temperature-Depth (CTD providing temperature/salinity profiles), TAO/TRITON/PIRATA/RAMA moorings (both temperature/salinity profiles), Argo profilers (both temperature and salinity profiles), Autonomous Pinniped Bathythermograph (APB providing both temperature and salinity fields). For the past data covering the period from 1957 until January 2010, quality-controlled profiles with depth correction factors were applied to XBT data. Operational GTS data is being used from January 2010 onwards. Sensitivity of SST products were fixed based on the standard deviation and inherent background errors, prescribing appropriate weights to observations in near shore regions, relevant corrections in the bias etc. ORAS4 data is an assimilated product that used bias corrected temperature and salinity profiles from various instrument sources. The assimilation procedure used bias correction scheme to correct the forcing errors in generating the ORAS4 datasets. More details pertaining to evaluation of ORAS4 are available in the study by Balmaseda et al. (2013) and the data assimilation procedures in Mogensen et al. (2012).

The ORAS5 belongs to the fifth-generation ocean reanalysis system developed at ECMWF based on ORAP5 (Zuo et al. 2015). ORAS5 includes five ensemble members and covers the period from 1979 onwards. It is regarded as a global eddy-permitting ocean ensemble reanalysis product. Both the forcing fields and observational datasets are updated in ORAS5. The novelty in ORAS5 is the application of generic ensemble generation scheme for perturbing both observations and forcing fields, ensemble-based spin-up time and the bias correction schemes. As compared to ORAS4 product, the ORAS5 showed an improved ocean climate variability in terms of SST and sea-level verified against independent observational datasets. As compared to ORAS4, the ORAS5 had a longer spin-up using reanalysis

for the period 1958–1979 using ERA40 and ERA20C forcing and in situ data assimilation.

The OHC fields derived from ORAS4 and ORAS5 at four sub-domains shown in Fig. 1 were used to estimate the OHC and also used for further analysis. Further, the Research Moored Array for African-Asian-Australian Monsoon Analysis and Prediction (RAMA) buoy data (McPhaden et al. 2009) was also used in the present study. The array in IO sector has a total of 16 moorings, of which 6 moorings are along the 90° E longitude, one each at 68° E and 95° E, five along 80° E, and array of three along 55° E longitudes. Data from RAMA buoys at three mooring locations were used to estimate OHC along the northern, central and southern regions. The findings obtained for these sub-domains are discussed in detail in the following section.

4 Results and discussion

4.1 Climatological distribution of SST over four sub-domains in BoB Basin

The Sea Surface Temperature (SST) is one of the most important parameters that help to understand the phenomena of deep atmospheric convection in tropical oceans (Bony et al. 1997). Further, a rise in SST can lead to an increase in vapour pressure saturation that triggers latent heat and leads to cyclone intensification. The climatological distribution of annual mean SST along four sub-domains during post- and pre-monsoon periods are shown in Figs. 2 and 3 respectively. More details on the selected locations marked as 'a', 'b',…, 'e' in Fig. 1 are tabulated in Table 3 for both the seasons. Each sub-domain marked 1–4 (Fig. 1) in the Bay of Bengal region has a spatial resolution of ~500 km × 500 km. For each representative box, the analysis was performed at five locations 'a', 'b', 'c', 'd', and 'e' that represents the four corner points and the box centre. The purpose behind selection of five points in each sub-domain is keeping in view the large spatial area under consideration for a detailed analysis in each sub-domain. SST variability analysis at these sub-domains provides an excellent test bed to further investigate the influence and role of oceanic thermal fields in the formative stages of tropical cyclogenesis.

Preliminary analysis of the results (Figs. 2 and 3) indicate that the climatological SST trends closely follows the climatological SST obtained from daily data of 3-day running mean TMI (TRMM Microwave Imager) and HYCOM MR (Main Run) with horizontal resolution of 0.25°·0.25° reported by Li et al. (2017). As seen from Fig. 2 and Table 3, the highest inter-annual variability is during the pre- and post-monsoon seasons for sub-domain 1 that corresponds to the northern Bay, followed by sub-domain 2 in the central Bay. The variability is also high during pre-monsoon
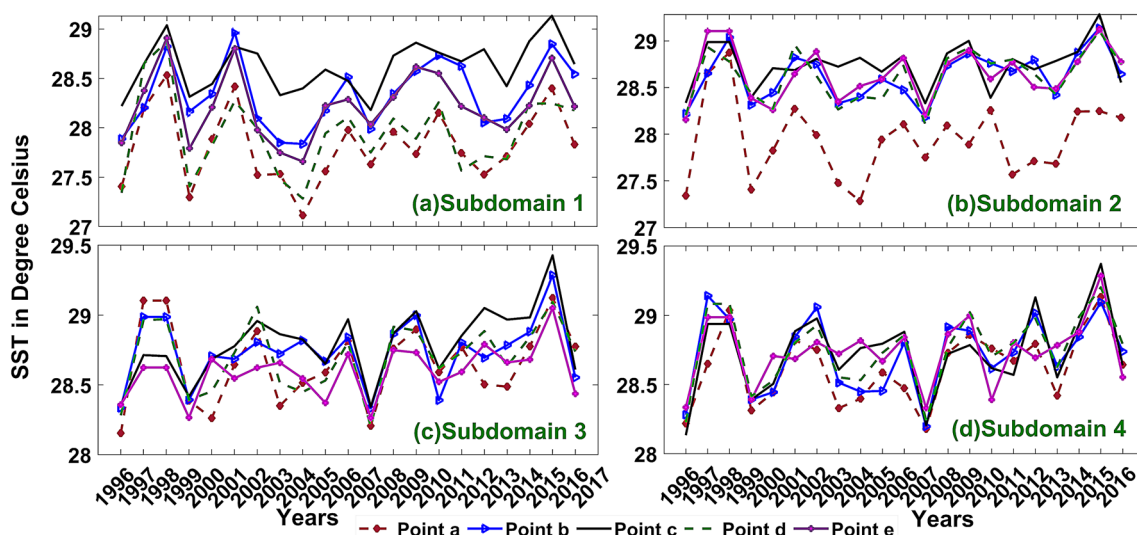
Fig. 2 Time-series distribution of SST (in °C) for all the four sub-domains: top-left panel for sub-domain 1, top-right panel for sub-domain 2, bottom-left for sub-domain 3, and bottom-right for sub-domain 4. In each panel the SST distribution for all five points with each sub-domain are shown during the post-monsoon season

in southern Bay, and in addition a contrasting difference is noticed during pre- and post-monsoon seasons. Interestingly, the inter-annual SST distribution exhibits a pentadal oscillation in these sub-domains warranting a separate detailed study, wherein the variability noticed in sub-domains 1 and 2 are different as compared to 3 and 4 respectively located in the southern and eastern boundary.

4.1.1 Pre- and post-monsoon SST variability

For the post-monsoon season (Fig. 2), the general SST pattern and trends at all four sub-domains representing the north, central, eastern, and southern regions in BoB showed a similar distribution. At sub-domains 1 and 2 (northern and central Bay) there was an indication of a 2-year cycle with gradual SST build-up (1996–1998; 1999–2001), followed by a drop (1998–1999; 2001–2004) respectively. At sub-domains 1 and 2, the SST minima were during 2004. The general observation is that during the study period 1996–2016, the SST exhibited an overall increasing trend with an accelerated increase from 2004 onwards having distinct increasing/decreasing cycles as mentioned above.

During pre-monsoon season (Fig. 3), in sub-domain 1 (northern Bay) the successive cycle of decreasing and increasing trend in SST ranged between 1- and 4-year duration during the study period, however, the trend accelerates from 2014 onwards. It is also evident that an accelerated positive SST trend is more distinct over sub-domains 3 and 4 (southern and eastern Bay) from 2008 onwards. The SST maxima in all sub-domains occurred during 2010, followed by distinct oscillatory cycle and accelerated trend.

4.1.2 SST variability trend over selected locations in the sub-domains

Trend analysis on SST variability for the five selected points (Table 3) at each sub-domain for 21 years (1996–2016) reveals that during post-monsoon the highest variability was observed in the southern Bay (corresponding to location '*c*' in sub-domain 3). Regions in the central (corresponding to locations '*b*' and '*e*' in sub-domain 2) and eastern Bay (corresponding to locations '*a*', '*c*' and '*e*' in sub-domain 4) also experienced high variability. Analysis for the pre-monsoon (Fig. 3) indicates highest SST variability in sub-domain 4, the eastern Bay region (Table 3). For this region, a warming bias was noticed with an increase in SST by about 0.89 °C as compared to the base year 1996 (Table 3). On an inter-annual scale, the SST variability at representative points is higher in the central and eastern bay (sub-domains 2 and 4) along the western side of the sub-domains. In general, it is observed that warming bias during the pre-monsoon season at sub-domain 1 (northern Bay) is much higher (almost double) as compared to the sub-domain 4 (eastern Bay).

4.1.3 Spatial distribution of SST anomaly

Figure 4 shows the spatial distribution of SST anomaly in BoB during the pre- and post-monsoon seasons. The divisions marked in this figure correspond to the four sub-domains representing northern, central, southern, and eastern regions of the Bay (Fig. 1). In general, the spatial distribution of SST anomaly during post-monsoon is higher as compared to the pre-monsoon season. Regions over sub-domain 1 (northern Bay) has the lowest SST anomaly

Table 3 SST variability during the pre- and post-monsoon seasons

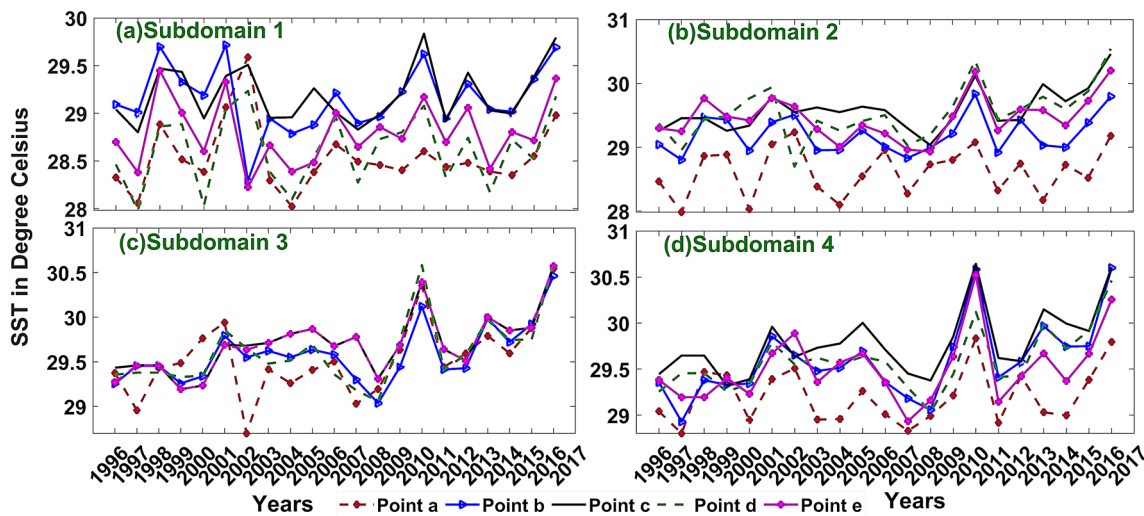| Data	Sub domain	Pre-monsoon SST (1996–2016)					Post-monsoon SST (1996–2016)				
		Min. SST (°C)	Max. SST (°C)	Δ SST (°C)	Mean SST (°C)	Trend slope (°C per year)	Min. SST (°C)	Max. SST (°C)	Δ SST (°C)	Mean SST (°C)	Trend slope (°C per year)
ERA-Interim	1	29.01	30.67	1.66	29.84	a 0.001 b 0.007 c 0.011 d 0.011 e 0.007	28.34	30.05	1.71	29.19	a 0.006 b 0.014 c 0.015 d 0.001 e 0.006
	2	30.68	31.16	0.48	30.92	a 0.011 b 0.011 c 0.029 d 0.035 e 0.015	29.77	30.13	0.36	29.95	a 0.001 b 0.015 c 0.008 d 0.009 e 0.015
	3	31.07	31.22	0.15	31.15	a 0.035 b 0.029 c 0.035 d 0.033 e 0.038	30.06	30.23	0.16	30.15	a 0.009 b 0.008 c 0.021 d 0.012 e 0.011
	4	30.50	31.39	0.89	30.95	a 0.011 b 0.038 c 0.033 d 0.029 e 0.022	30.05	30.34	0.29	30.19	a 0.015 b 0.010 c 0.014 d 0.008 e 0.014

Fig. 3 Time-series distribution of SST (in °C) for all the four sub-domains: top-left panel for sub-domain 1, top-right panel for sub-domain 2, bottom-left for sub-domain 3, and bottom-right for sub-domain 4. In each panel the SST distribution for all five points with each sub-domain are shown during the pre-monsoon season

Fig. 4 Spatial distribution of SST anomaly (in °C) generated using the difference between long-term monthly average and corresponding data for the base period (1996–2016) during **a** pre-monsoon, and **b** post-monsoon seasons in the Bay of Bengal
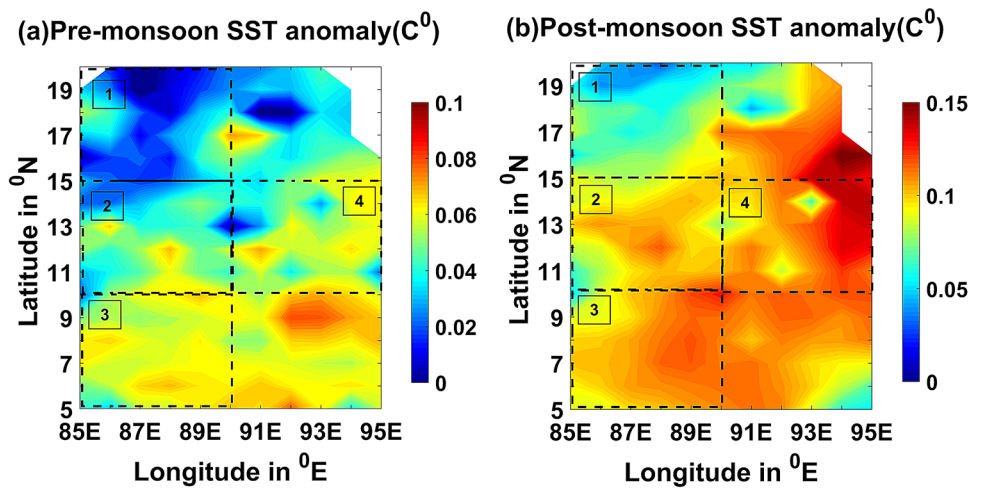

especially during pre-monsoon, and that is relatively higher in the post-monsoon season. Regions in the same latitudinal belt (sub-domain 1) at the eastern side during post-monsoon season exhibit higher anomaly almost comparable to other sub-domains in the study area. These findings are analogous with the observed SST variability over all sub-domains and trends at each location (Figs. 2 and 3, and Table 3).

4.2 SST correlation with naximum sustained wind speed (V_{max}) of cyclones

Figure 5 shows the correlation between maximum sustained wind speed against SST for all the sub-domains during pre- and post-monsoon seasons. In general, the pre-monsoon mean SSTs are higher as compared to the post-monsoon

season. In terms of intensity; the post-monsoon cyclones have higher V_{max} as compared to pre-monsoon cyclones. Interestingly, the correlation between SST and V_{max} is clustered over a larger SST range for pre-monsoon cyclones as compared to post-monsoon cases, in particular for the sub-domains 3 and 4. Results indicate a weak correlation less than 0.3 between maximum sustained wind speed and SST for the pre-monsoon cyclones Differential water mass characteristics influenced by complex ocean circulation features and varying hydrological influx can lead to seasonal variations in the best-fit trend noticed at central Bay (sub-domain 2) and northern Bay (sub-domain 1) during the pre- and post-monsoon seasons. Routine in situ measurements conducted over time clearly indicate a rising trend in the SST and sub-surface temperatures over the Bay region (Sahoo

Fig. 5 Correlation between maximum sustained wind speed (Vmax) for all categories of cyclonic storms that formed during 1996–2016 against SST corresponding to the genesis location for **a** pre-monsoon, and **b** post-monsoon seasons in all the four sub-domains
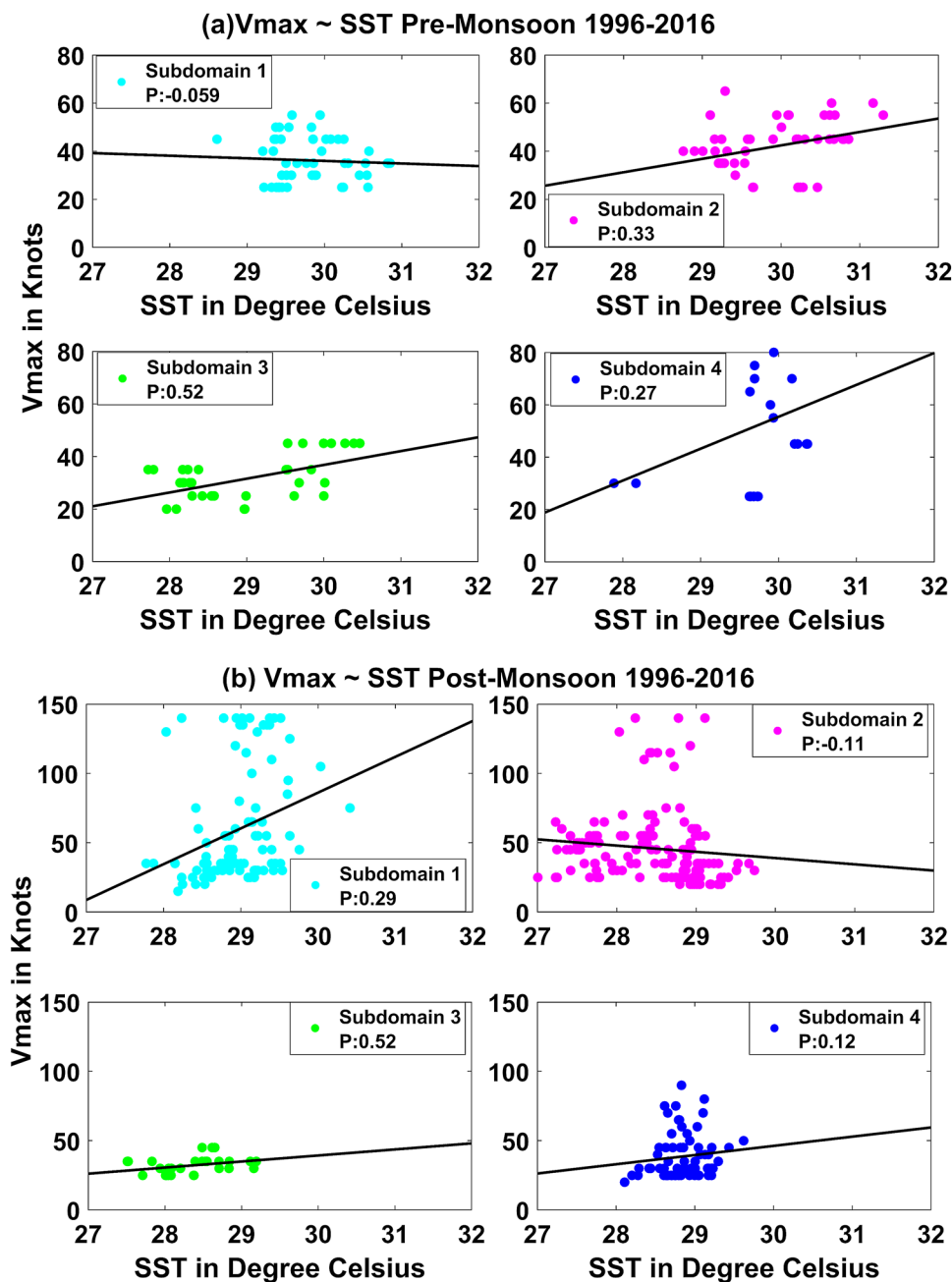
and Bhaskaran 2016). During recent years, this region had also experienced high intense cyclonic events unlike the past decades, and in-phase correlation is seen between SST and V$_{max}$ during the study period. The relationship is negatively correlated for the northern head Bay (sub-domain 1 in Fig. 1) during pre-monsoon season, whereas a weak positive correlation is seen during the post-monsoon season. The central Bay (sub-domain 2 in Fig. 1) region has a weak positive correlation during pre-monsoon, whereas it is negatively correlated during the post-monsoon season. The relationship is positively correlated for sub-domains 3 and 4 (southern and eastern Bay) both during pre- and post-monsoon

seasons, exhibiting a highest correlation about 50% for subdomain 3 during the post-monsoon season.

Ali et al. (2013) investigated the relationship between cyclone intensities and SST for the tropical Indian Ocean region. Out of 75 cyclones cases considered during 1998–2011, their study revealed that more than 50% of cyclones have no significant correlation between cyclone intensities and SST, indicating that SST is not a useful indicator for cyclone intensities in the tropical Indian Ocean. These observations are in close agreement that show the dependency of maximum sustained wind speed (V$_{max}$) against SST depicted in Fig. 5 for the pre- and post-monsoon

seasons in BoB. Analysis of SST from ERA-Interim dataset indicates that the basin-scale SST anomaly at all four sub-domains varied between 2° C (maximum) and 1.7 °C (minimum) during the post-monsoon season, whereas the variability was 2.4° C (maximum) to 1.6° C (minimum) during pre-monsoon season (Table 3). These results indicate that maximum variability (difference in maxima-minima) is for the sub-domain 1 (Fig. 1) as compared to the other sub-domains. A closer introspection and analysis of OHC is warranted, and their trend requires a detailed evaluation along with SST in order to understand the thermodynamic cycle on tropical cyclone intensification in a better perspective.

4.3 Ocean heat content variability analysis using ORAS4 and ORAS5

To explore the variability of sub-surface temperatures in the Bay region, an inter-comparison exercise was carried out between the three RAMA buoys (shown in Fig. 1) against the ECMWF Ocean Reanalysis System ORAS4 and ORAS5 datasets (Fig. 6). This mutual comparison between datasets would be useful to estimate and assess the variability of OHC and its influence on the development and evolution of tropical cyclogenesis. Balmaseda et al. (2013) reported on the performance of ORAS4 showing a clear and robust nonlinear trend in the 0–700 m OHC consistent with observational estimates. The reanalysis products ORAS4 (Balmaseda et al. 2013) and ORAS5 (Zuo et al. 2015) used in this study incorporates the quality-controlled ERA-Interim forcing fluxes, with necessary multi-scale bias corrections applied on XBT and Argo datasets, revised ensemble generation techniques, generic ensemble generation schemes, ensemble-based spin-up time to better represent the uncertainty in deeper oceans. Keeping in view the best available dataset for the present study, the data quality of ORAS4 and ORAS5ensures its utilization and justification for

understanding OHC variability in the BoB basin. The top layer of 300 m (D_{300}) was chosen in this study for the estimation of OHC utilizing both ORAS4 and ORAS5data.

4.3.1 Validation with RAMA buoy observations

As seen from Fig. 6, the validation between the two reanalysis products against in situ observations looks satisfactory from 2010 onwards. It could be attributed to the dense network of in situ observations such as Argo floats that were used in the data assimilation procedure and subsequent bias correction techniques used to generate the reanalysis products. As an inter-comparison exercise, this study also estimated the statistical quantities such as the RMSE (Root Mean Square Error) and MPD (Mean Percentage Deviation) between ORAS4 and ORAS5 against the RAMA buoy data (Fig. 6). Lower values of RMSE indicate a better fit between both ORAS4 and ORAS5 against the in-situ RAMA buoy observation. The MPD for ORAS4 varied from 4.01 to 6.17% and the same for ORAS5 was from 3.91 to 5.49%. In general, lower values for both RMSE and MPD indicates a better fit with the observational data. This validation exercise shows that the performance of both ORAS4 as well as ORAS5 is satisfactory at the three buoy locations. However, based on the estimated statistical measures it is clear that ORAS5 is relatively better as compared to the ORAS4 product.

4.3.2 Seasonal anomaly of OHC

Figure 7 represents the seasonal anomaly of OHC for the 0–700 m water depth (D_{700}) covering a period of 64 years (1955–2018) for the global ocean basins (Source: Time series data from NOAA-World Ocean Database: Global Ocean Heat and Salt content). As seen from this figure, the highest warming trend is evidenced for the Atlantic Ocean

Fig. 6 Time-series comparison of Ocean heat content (in J/m²) between ORAS4, ORAS5, and RAMA buoys along the 90° East transect in the Bay of Bengal
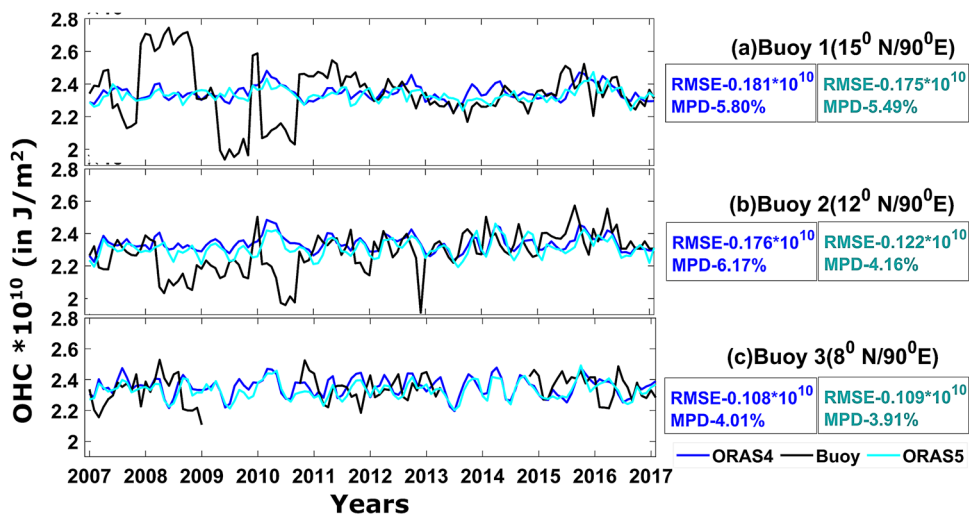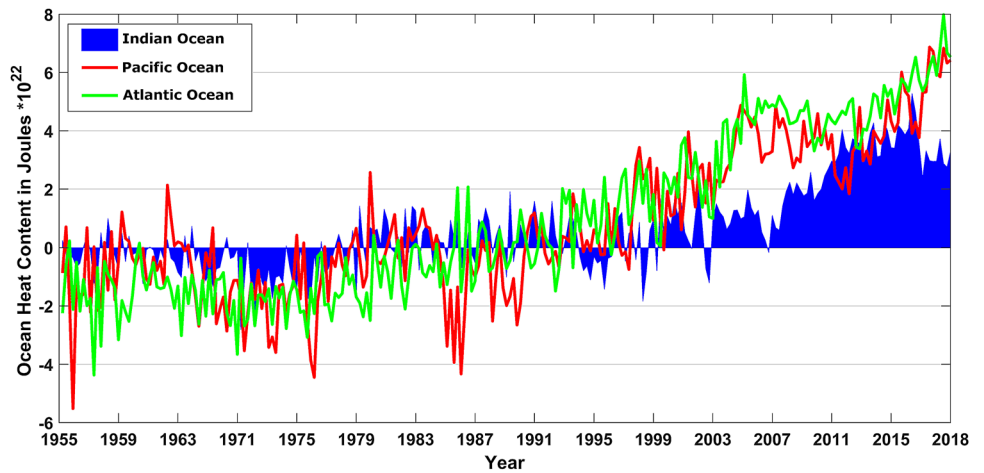
Fig. 7 Seasonal anomaly of Ocean heat content integrated from surface to 700 m water depth for the period 1955–2018 in the global ocean basins

followed by the Pacific and Indian Ocean basins. A clear warming trend is noticed for all the three ocean basins from 1975 onwards, with an accelerated rise from 1991 onwards. Recent OHC anomalies(D_{700}) for the Atlantic, Pacific, and Indian Ocean basins are 8×10^{22} J; 6.5×10^{22} J; and 3×10^{22} J respectively. Though an accelerated rise in OHC anomalies are noticed for the Atlantic and Pacific Ocean basins since 1991, the present decade for the Indian Ocean basin from 2007 to 2016 showed an accelerated rise in seasonal OHC anomaly along with intermediate cooling episodes. These findings indicate that an in-depth comprehensive analysis is warranted on OHC variability for the Indian Ocean basin in particular for the pre- and post-monsoon months. The spatial distribution of OHC anomaly during pre- and post-monsoon seasons is shown in Fig. 8. It provides valuable information on the variability of OHC anomaly at various sub-sectors in the BoB basin. The divisions along with the boxes numbered in

this figure correspond to the four sub-domains representing northern, central, southern, and eastern regions of the Bay. In general, it is noticed that the spatial distribution of OHC anomaly during pre-monsoon is higher as compared to the post-monsoon season, unlike the distribution of SST anomaly shown in Fig. 4. The OHC anomalies for regions in sub-domain 1 (northern Bay) is relatively lower during post-monsoon as compared to the pre-monsoon season. However, for the same region, the SST anomaly was relatively lower in pre-monsoon as compared to the post-monsoon season (Fig. 4). The maximum/minimum variations in positive/negative OHC anomaly was noticed at sub-domains 2 and 4 respectively during the post-monsoon season. Interestingly, the contrasting differences in positive (negative) anomalies are noticed over the southern Bay (sub-domain 3) during pre- and (post-monsoon) seasons respectively having potential implications on tropical cyclogenesis and intensification in the BoB basin.

Fig. 8 Spatial distribution of Ocean heat content Anomaly ($\times 10^7$ J) generated using the difference between long-term monthly average and corresponding data for the base period (1996–2016) during **a** pre-monsoon, and **b** post-monsoon seasons in the Bay of Bengal
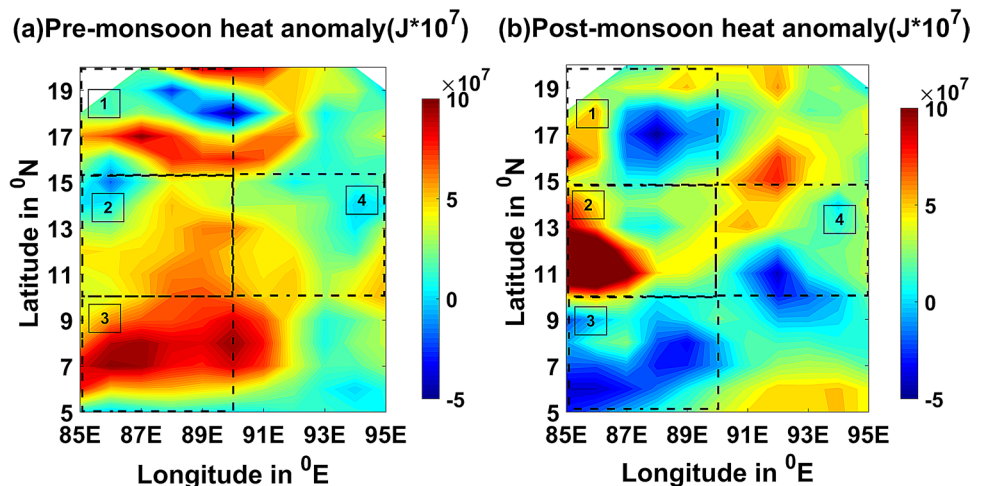
4.3.3 OHC variability at RAMA buoy locations and sub-domains

Further a detailed analysis was carried out to understand the OHC variability utilizing both ORAS4 and ORAS5 data for the upper 300 m (D_{300}) water depth for the study period (1996–2016). Figure 9 shows the time-series comparison of OHC between ORAS4 and ORAS5 at the three RAMA buoy locations (Fig. 1) representing the northern, central, and southern Bay regions. As seen from this figure, the trends in general exhibited by ORAS4 are relatively higher as compared to ORAS5 at all three RAMA buoy locations. Highest variability is seen at northern Bay region corresponding to the buoy location (15° N, 90° E) almost 35% higher with reference to ORAS5. This difference reduces to 9% and 7% respectively at the central and southern Bay regions. Taking into consideration the data quality of ORAS5 which is an upgraded product as compared to ORAS4, the highest trend is noticed at central Bay region showing an increase of

about 1.73×10^6 J/year followed by the northern Bay (1.67×10^6 J/year). Similar trend analysis for each sub-domain (Fig. 10) indicates that sub-domain 4 located in the eastern Bay (Fig. 10d) experiences highest OHC variability (~ 1.25×10^6 J/year) followed by sub-domain 3 (Fig. 10c) in the southern Bay (~ 1.2×10^6 J/year). The OHC build-up is relatively lower for the sub-domain 1 (Fig. 10a~ 1.1×10^6 J/year). In general, all sub-domains showed an increasing trend in the OHC variability.

Table 4 provides more details on the OHC trend distribution at locations (*a–d*) along the four sub-domains (Fig. 1). The annual maxima-minima for all sub-domains is relatively higher in ORAS4 as compared to the ORAS5 product, and that is reflected in the estimated trends at all sub-domains, however with an exception for the sub-domain 4 (eastern Bay). Jangir et al. (2019) performed an inter-comparison between model, satellite and in situ TCHP for the NIO. It used INCOIS-GODAS model and satellite derived TCHP data against estimated TCHP from in situ profiles comprising

Fig. 9 Time-series comparison of Ocean heat content between ORAS4 and ORAS5 for the upper 300 m ($\times 10^{10}$ J/m^2) at the three RAMA buoy locations representing the **a** northern Bay, **b** central Bay, and the **c** southern Bay
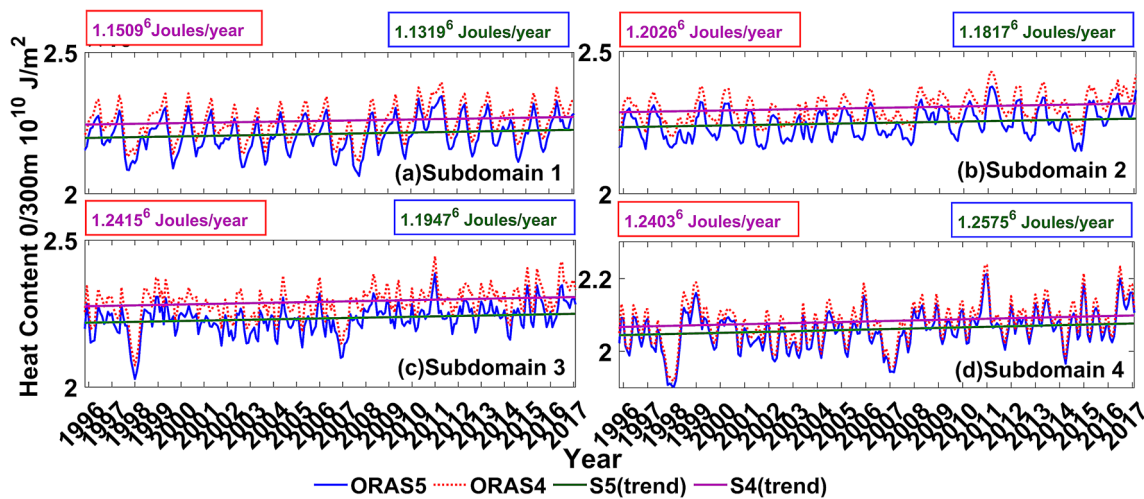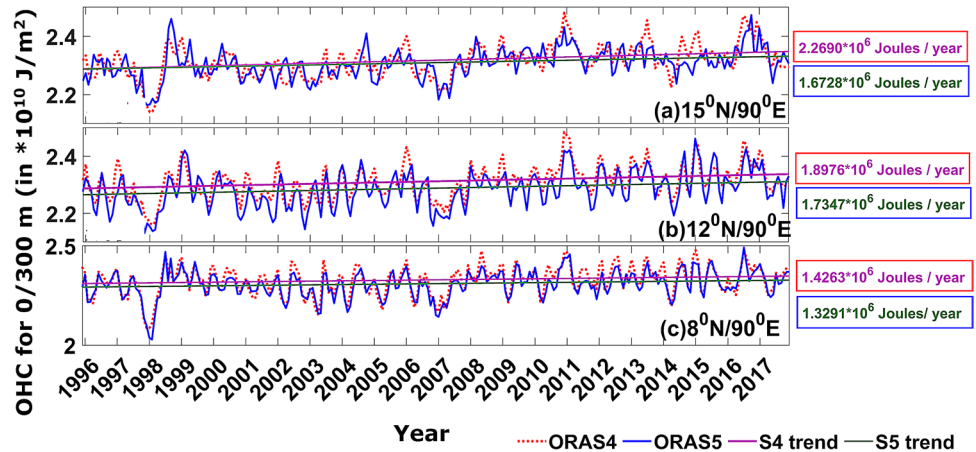

Fig. 10 Time-series distribution of Ocean heat content (in $\times 10^{10}$ J/m^2) between ORAS4 and ORAS5 for the upper 300 m water depth and their trends at the four sub-domains

Table 4 OHC trend values at locations (a–d) for each sub-domain (1–4)

Sub-domain	Point	Trend ($\times 10^6$ Joules per year)
1	a	0.755
	b	3.32
	c	2.85
	d	1.76
2	a	1.76
	b	2.85
	c	2.86
	d	2.88
3	a	3.32
	b	3.76
	c	3.48
	d	2.85
4	a	–
	b	3.99
	c	3.32
	d	0.755

of eight moored buoys during 2011–2013 and 2005–2015 with Argo data. A reasonably good correlation was seen for the statistical measures between model and in situ TCHP (Jangir et al. 2019). It compared model and in situ TCHP for *Thane* cyclone at two buoy locations. Comparison of TCHP on seasonal scale with in situ estimated TCHP showed better correlation for the pre- as compared to post-monsoon season. Influence of eddies and TCHP on changes in tropical cyclones intensification over NIO basin was recently reported by Jangir et al. (2020). Sea level data from AVISO, satellite based TCHP and cyclone intensity data from IMD were used to understand the impact of TCHP and eddies for 60 cyclone cases (38 in BoB, and 22 in Arabian Sea) between 2001 and 2018. Analysis revealed that almost 40% cyclones are influenced by warm core eddy playing a role in intensification, whereas 30% are influenced by cold core eddy that reduces intensification, and the remaining 30% are influenced only by TCHP variations. Those cases that do not follow the established trend are primarily governed by the translation speed. Anandh et al. (2018) studied the OHC during 1980–2014 for the BoB region. Their study analyzed the Reanalysis of Simple Ocean Data Assimilation (SODA) and ECMWRF-ORAS4 datasets to estimate the OHC and heat flux. Their results indicated that storage of heat energy is centred over southern and north-western Bay region with an increasing trend. Analysis showed that incoming heat flux for the eastern side showed a significant increase from 0.18×10^{12} W/month to 0.57×10^{12} W/month (Anandh et al. 2018). Their study also pointed out considerable loss in outgoing heat flux along western side of the basin. An imbalance between incoming and outgoing heat flux is the responsible factor that contributes to increase OHC in the Bay region. Findings in the present study are analogous with Anandh et al. (2018) indicating higher OHC variability over the northern and southern Bay regions (shown in Fig. 8). An interesting feature noticed from this study is along the longitudinal transect (spatial extent covering the southern to northern boundary of Bay region) the annual OHC variability showed about 35% increase that is quite substantial in context to tropical cyclogenesis.

4.4 Meridional mean anomaly variation of OHC and SST over Bay of Bengal

Meridional mean time evolution of seasonal anomalies pertaining to SST and OHC for the study region represented as Hovmöller plots are shown in Fig. 11. A closer examination on the spatial gradients for SST anomaly shown in Fig. 11a, b respectively for the pre- and post-monsoon seasons indicate an oscillatory nature having episodes of alternate warm and cold bias events for the study period. During the pre-monsoon season (Fig. 11a), a distinct warm bias is noticed for the entire BoB during 1998–1999 more pronounced along the western side, and that was followed by a cold bias event on the eastern side during 2000. The study reveals successive cycle of warm and cold bias events in the study region (Fig. 11a) with distinct spatial variability during certain years. As seen, 2005–2006 experienced a warm bias for the entire basin followed by intense cooling during 2007–2008. It is noteworthy that intense warming covered the entire basin during 2015–2017.

Seasonal SST anomaly distribution for post-monsoon (Fig. 11b) also showed warming and cooling episodes. Spatial variations observed during 1997–2000 had a close similarity with observed trends in the pre-monsoon season (Fig. 11a). An interesting point is during the post-monsoon season from 2000 onwards, wherein the spatial variability of SST anomaly reveals prolonged warming unlike the observed trends during pre-monsoon season. In general, the study signifies that warming dominates the cooling episodes for the entire BoB basin (Fig. 11b). It is worth noting that intense warm bias build-up during 2014–2015 (Fig. 11b) is also reflected in the pre-monsoon season of succeeding year 2015–2016 (Fig. 11a). Interestingly, the pre- and post-monsoon seasonal OHC anomaly (Fig. 11c and d) during 1997–2000 had a close similarity with warming bias over the western Bay region with an opposite polarity between seasonal OHC and SST anomalies (Fig. 11a, b). The SST anomaly showed warming during 2002–2003 (Fig. 11a), whereas the OHC anomaly showed cooling (Fig. 11c). The warming episode is found extending for rest of the years (Fig. 11c) from 2007 onwards, unlike the observed trend in SST anomaly (Fig. 11a). These observations are quite unique, and it is quite obvious that in recent years the sub-surface waters

Fig. 11 Hovmoller diagram representing the meridional mean (averaged between 5° N and 20° N) corresponding to the **a** pre-monsoon season SST anomaly, **b** post-monsoon season SST anomaly, **c** pre-monsoon season OHC anomaly, and **d** post-monsoon season OHC anomaly
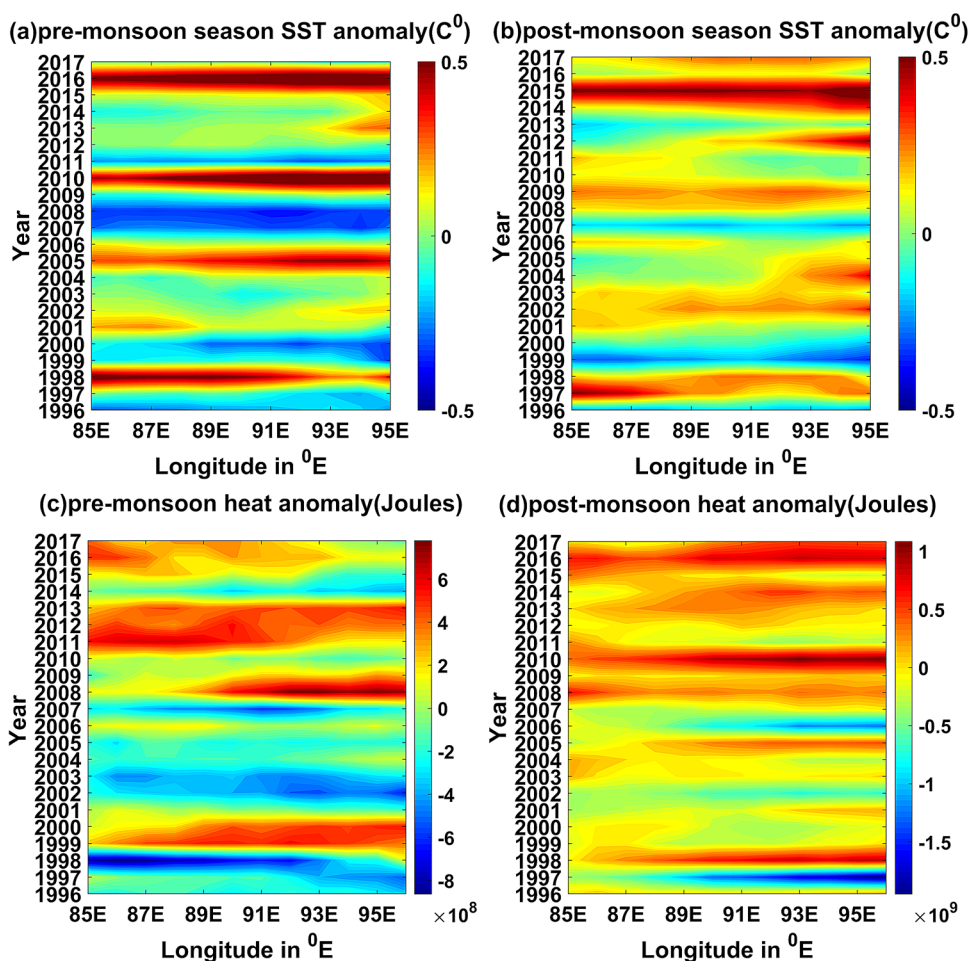
are turning warmer and that has direct relevance in context to tropical cyclogenesis. The findings reveal that there are strong seasonal variations; however, there is an upward trend in both SST and OHC anomalies with time. Interestingly, the warming trend is noticed to dominate basin-wide during the pre-monsoon season, and since 2007 the post-monsoon seasonal OHC anomaly continued to warm over the entire Bay having direct implications on tropical cyclone activity and storm intensification.

## 4.5 OHC variability and cyclone characteristics over BoB

4.5.1 Basin scale distribution of OHC anomaly and cyclone frequency

The time series distribution concerning basin-scale distribution of OHC anomaly and the total frequency of cyclones for BoB basin are shown in Fig. 12. Analysis reveals an increasing trend with a net increase of 0.643 J/m^2 during the study period. Decreasing trend in the OHC anomaly was evident during 1996–1998, with a largest dip during 1998.

Thereafter, no distinct trend was observed until 2004. The period 1996–2000 experienced negative OHC anomaly, and thereafter sustained positive OHC anomaly was maintained. An accelerated increasing trend was observed in the OHC anomaly from 2004 onwards.

In a broader perspective, marginal decline was noted in the total frequency of cyclones during the study period (22.1%). The category of SCS + VSCS and DD are analogous with the general trend of declining pattern with a percentage change of − 14.7% and − 14.58% respectively. However, the CS category showed an increasing trend with a noticeable change of 46.66%. The highest frequency of cyclones was during 2005–2007 and 2013. Even though the frequency of total cyclones marginally declined during the recent decade with an exception for 2013, the rise is steady during 2014–2016, and there are evidences supporting a greater number of high intense storms of CS category are increasing over the BoB region. As per the records of India Meteorological Department (IMD), for the BoB basin during 1996–2016, a total of 125 events were reported that includes depression (D), cyclonic storms (CS), and severe cyclonic storms (SCS). The total number of D, CS, and SCS were

Fig. 12 Time-series distribution of Ocean heat content Anomaly (in J/m^2) for the upper 300 m water depth in the Bay of Bengal basin and corresponding total frequency of cyclones grouped into SCS + VSCS (in pink), CS (in green), and DD (in brown) along with their trends and % change of individual cyclone category
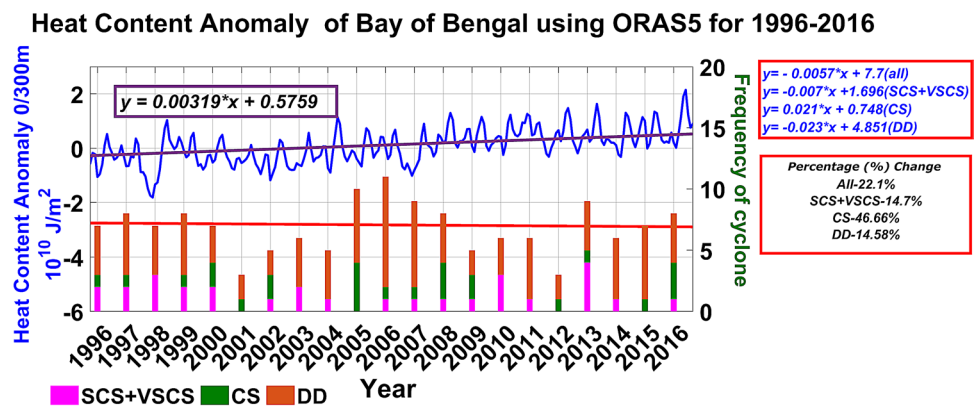
72, 24, and 29 respectively. For the sub-domains numbered 1–4 (Fig. 1), the total number of D, CS, and SCS were 54, 29, and 15 respectively (Table 1). Considering the entire Bay region, the probability of intensification from D stage to CS was 72.2%, from D to SCS was 44.4%, and from D to CS to SCS was 61.5% during the pre-monsoon season. Similarly, during the post-monsoon season, the probability of intensification for stages from D to CS, D to SCS, and from CS to SCS were 56.7%, 33.3%, and 58.8% respectively. Annual percentage probability of intensification from D to CS, D to SCS, and from CS to SCS was 42.4%, 23.2%, and 54.7% respectively. As seen from these statistics, this study clearly postulates that with an increasing trend evidenced in SST and OHC, the annual percentage probability of tropical cyclone intensification is also found higher (54.7%) for stages that transform from CS to SCS. The study also finds an increasing trend in the occurrence frequency of CS category for the base period (1996−2016) over BoB basin (Fig. 12). The highest annual percentage of intensification is for CS to SCS category. Annual percentage probability of intensification shows an upward trend from CS to SCS stage for the base period (1996−2016).

4.5.2 Influence of OHC on BoB Cyclone Intensification

The analysis of OHC anomaly and frequency of cyclones as shown in Fig. 12 clearly indicate that the shift from cooling to warming bias in OHC anomaly is evident from 2004 to 2005 (negative to positive shift). Also, the frequency of tropical cyclone events was maximum during the period 2005–2007 and 2013. In order to evaluate cyclone intensification and its influence by positive phase of OHC anomaly, the study considered only cyclones for the period 2006–2016. This study also examined the role and influence of OHC on different cyclonic cases that developed and intensified in the BoB basin during the period 2006–2016. More details regarding the cyclones categorized based on pre- and post-monsoon seasons and grouped under different stages from genesis to intensified storms at various sub-domains

of the study region are shown in Table 5. Out of the total 18 cyclones considered, there are 11 post-monsoon and 7 pre-monsoon cases. For post-monsoon cyclones, out of 11 events the genesis locations of 8 cyclones are in sub-domains 3 (southern Bay) and 4 (eastern Bay), while 3 of them are in the sub-domain 2 (central Bay). These genesis locations exhibited a strong correlation with the post-monsoon SST anomaly (Fig. 4). There are six cases that intensified from D to CS category and their locations correspond to sub-domain 4 (eastern Bay) while three of them are at sub-domain 2 (central Bay). Higher intense category from CS to SCS, has six cases in sub-domain 2 (central Bay) and one case in sub-domain 4 (eastern Bay). Extremely intense category that transformed from, SCS to VSCS/ESCS show four cases in sub-domain 2 (central Bay) and three cases in sub-domain 1 (northern Bay).

The study reveals that majority of the intensified cases are in sub-domain 2 (central Bay) that corresponds to highest OHC anomaly during the post-monsoon season (Fig. 8) and also matches with the trend (Fig. 9b) estimates from ORAS5. Also, none of the intensified cases during pre- and post-monsoon seasons are reported in sub-domain 3 (southern Bay) that witnessed the lowest/highest OHC anomaly (Fig. 8; Table 5). For pre-monsoon cyclones, out of 7 events the genesis locations of 2 cyclones are in sub-domains 3 (southern Bay), 3 in central Bay, and 1 in sub-domain 1 (northern Bay). Also, it is seen that these genesis locations have a strong correlation with the pre-monsoon SST anomaly (Fig. 4a). Maximum number of post-monsoon cyclones had their genesis location in sub-domain 4 (eastern Bay), while there are no such cases seen for the pre-monsoon cyclones. For pre-monsoon cyclones, there are four cases that intensified from D to CS category and their locations correspond to sub-domain 2 (central Bay) while two of them are at sub-domain 1 (northern Bay) and one at sub-domain 4 (eastern Bay). Higher intense category from CS to SCS, had a total of one each in sub-domains 1, 2, and 4. Further, extremely intense cyclone category from SCS to VSCS/ESCS had one each in sub-domains 1 and 4.

Table 5 Pre- and Post-monsoon cyclonic events that developed over the NIO basin grouped under different stages in various sub-domains

Year	Pre/Post-Monsoon	Cyclone Name	Sub-domains (1–4)			
			Genesis	DD-CS	CS-SCS	SCS-VSCS/ESCS
2016	Post-Monsoon	*Vardah*	3	4	2	2
2016	Post-Monsoon	*Nada*	3	2	–	–
2016	Post-Monsoon	*Kyant*	2	4	–	–
2016	Pre-Monsoon	*Roanu*	-	4	–	–
2014	Post-Monsoon	*Hudhud*	4	4	2	1
2013	Post-Monsoon	*Madi*	Near 2	Near 2	2	1
2013	Post-Monsoon	*Lehar*	4	4	4	2
2013	Post-Monsoon	*Helen*	2	1	–	–
2013	Post-Monsoon	*Phailin*	4	4	2	1
2013	Pre-Monsoon	*Viyaru*	3	2	–	–
2012	Post-Monsoon	*Nilam*	3	–	–	–
2011	Post-Monsoon	*Thane*	3	2	2	Near 2
2010	Pre-Monsoon	*Laila*	2	2	–	–
2009	Pre-Monsoon	*Bijli*	2	1	–	–
2009	Pre-Monsoon	*Aila*	1	1	1	–
2008	Pre-Monsoon	*Nargis*	2	2	2	1
2007	Post-Monsoon	*Sidr*	4	4	2	2
2006	Pre-Monsoon	*Mala*	3	2	4	4

The study signifies that the central, eastern, and northern Bay regions favours the intensification of the pre-monsoon cyclones and they have a strong correlation with the OHC anomaly (Fig. 8a). This study confirms the fact that genesis locations have a strong correlation with SST anomalies both for the pre- and post-monsoon cases, as well the spatial gradients in OHC anomalies favours the intensification. Findings from the present study is analogous with Mawren and Reason (2016) who examined the variability of upper ocean characteristics for cyclones in the southwest Indian Ocean in the southern hemisphere indicating the role of OHC and thickness of barrier layer influencing tropical cyclone intensification. In addition, the tropical cyclone characteristics in the Indian Ocean is strongly influenced by barrier layer characteristics prominent over the northern Bay region, atmospheric steering that guides the pathway of cyclone translation, and funnelling effect of the Bay that steers the cyclone track. A separate detailed study is required on each of these aspects to better understand the tropical cyclone characteristics.

4.6 Tele-connection between OHC and ONI (Oceanic Niño Index)

4.6.1 ONI (Oceanic Niño Index)

Keeping in view the tele-connection between different ocean basins, the present study also explored the observed variability in OHC with possible tele-connections for events that trigger in the Pacific Ocean basin. Specifically, the study only focused on colder episodes (La Niña events) grouped under different categories such as Weak, Moderate, and Strong. The time series information of ONI (Oceanic Niño Index) categorized as weak, moderate, strong, and very strong cases of El Niño and La Niña events represented as a 3-month running mean for the period 1950–2019 are available from the URL link: http://www.cpc.noaa.gov/products/analysis_monitoring/ensostuff/ensoyears.shtml). The ONI is a standard by NOAA used to identify warm events (El Niño) and cold events (La Niña) in the tropical Pacific Ocean. It is based on a 3-month average SST anomaly for the Niño 3.4 region (5° N−5° S; 120°−170° W). Based on a five-consecutive overlapping of the 3-month periods the events are classified either as warm (+0.5° anomaly) or cold (-0.5° anomaly). Further, the threshold values are again classified as weak (for SST anomaly between 0.5−0.9), moderate (for SST anomaly between 1.0 and 1.4), strong (for SST anomaly between 1.5 and 1.9), and very strong ($\geq$ 2.0). Table 6 provides a more elaboration expressed in index on the respective strength of weak, moderate, strong, and very strong El Niño and La Niña events that provides an opportunity to corroborate the time series of OHC variability at RAMA buoy locations (Fig. 9).

Yoo et al. (2010) investigated the relationship between Indian Ocean SST and the transition of El Niño events into either La Niña or El Niño–Southern Oscillation (ENSO) neutral conditions using observations and ensemble hindcasts of NCEP CFS revealing a robust and consistent relationship with evolution of these transitions for the southern Indian Ocean region. Their study (Yoo et al. 2010) proposed

Table 6 Time series of Oceanic Nino Index (ONI) based categorization

El Nino				La Nina		
Weak	Moderate	Strong	Very strong	Weak	Moderate	Strong
1952–1953	1951–1952	1957–1958	1982–1983	1954–1955	1955–1956	1973–1974
1953–1954	1963–1964	1965–1966	1997–1998	1964–1965	1970–1971	1975–1976
1958–1959	1968–1969	1972–1973	2015–2016	1971–1972	1995–1996	1988–1989
1969–1970	1986–1987	1987–1988		1974–1975	2011–2012	1998–1999
1976–1977	1994–1995	1991–1992		1983–1984		2007–2008
1977–1978	2002–2003			1984–1985		2010–2011
1979–1980	2009–2010			2000–2001		
2004–2005				2005–2006		
2006–2007				2008–2009		
2014–2015				2016–2017		
2018–2019				2017–2018		

Table 7 Correlation between (Oceanic Nino Index) ONI and OHC300 values at buoy locations 1(B1), 2(B2), and 3(B3)

Year	Event[a]	B1 (15° N/90° E)	B2 (12.5° N /90° E)	B3 (8.5° N /90° E)
1996–1997	ML	0.23	0.32	0.46
1998–1999	SL	0.51	0.54	0.58
1999–2000	SL	0.74	0.84	0.83
2000–2001	WL	0.26	0.26	0.31
2005–2006	WL	0.38	0.43	0.57
2007–2008	SL	0.68	0.83	0.84
2008–2009	WL	0.40	0.49	0.46
2010–2011	SL	0.41	0.48	0.48
2016–2017	WL	0.35	0.42	0.60

[a]The Events ML, SL, and WL refers to Moderate La Niña, Strong La Niña, and Weak La Niña respectively

a physical mechanism that connects air-sea interaction process for the Indian and western Pacific Ocean basins. Based on observational evidences, the easterly surface wind anomalies in the western Pacific Ocean are associated with La Niña emergence during boreal summer and fall. These winds are also significantly correlated to SST in the southern Indian Ocean (Yoo et al. 2010).

4.6.2 Correlation between OHC and ONI

The above-mentioned studies indicate on the possible teleconnection between the strengths of El Niño and La Niña events in the Pacific Ocean and possible linkage to OHC in the Indian Ocean region. The current study focused on the colder events (La Niña) and its correlation with OHC for different categories like weak, moderate, and strong events. The correlation values are obtained for different La Niña events that occurred during 1996–2017 shown in Table 7. The correlation values are estimated at three RAMA buoy locations at 90 degree transect (B1, B2, and B3 in Fig. 1). This provides an opportunity to evaluate the correlation strength along the north-south transect of the Bay region.

As seen from Table-7, the period 1996–1997 corresponds to a Moderate La Niña (ML) and during this time the OHC exhibited an in-phase relation at all buoy locations B1(0.23), B2(0.32) and B3(0.46) in the increasing order of correlation value (Fig. 9). The OHC magnitude also increased relatively from north to south of the Bay region (B1 located at north and B3 at south). The period 1998–2000 corresponds to a Strong La Niña (SL) event, and during this period an in-phase relation is noticed with the OHC distribution. The corresponding correlation between ONI and OHC at buoy locations are: B1 (0.51, 0.74); B2 (0.54, 0.84); and B3 (0.58, 0.83) over the BoB (Table 7; Fig. 9) with a higher OHC magnitude as compared to 1996–1997. On the other hand, 2000–2001 was a Weak La Niña (WL) year which also showed an in-phase relation with OHC, however with weaker magnitudes. The corresponding correlation at the three buoy locations are: B1(0.26), B2 (0.26), and B3(0.31). A similar observation for WLs during 2005–2006, 2008–2009, and 2016–2017 are also reflected in the OHC distribution over the study region (Fig. 9). Strong La Niña (SL) events during 2007–2008 (B1: 0.68, B2: 0.83, B3: 0.84) and 2010–2011 (B1: 0.41, B2: 0.48, B3: 0.48) also showed an in-phase relation with higher magnitudes during 2010–2011. Higher magnitudes in OHC has a strong dependence with the 3-month running ONI for the BoB basin. A comprehensive study is warranted to understand the strength of specific events in the Pacific basin and the air-sea coupled mode IOD (Indian Ocean Dipole) events and its influence on the lead-lag time in OHC distribution which will be carried out in a detailed separate study. Further, the study also brings to light that in the present decade, there is substantial increase in the cyclone heat potential especially during the post-monsoon season that corroborates with present findings in the SST and OHC fields for the BoB region.

During the period 2000–2016, almost 50% of cyclones that developed during the post-monsoon season have intensified into severe cyclonic storms. Increased OHC levels are responsible for the occurrence of more severe cyclones in the recent years.

5 Conclusions

The oceans play a major role in global warming and a substantial fraction of heat is being transferred into the subsurface through convective processes, small scale eddies and large-scale circulation. The largest contributor to thermal inertia in the climate system also resides in the ocean supporting tropical cyclones through moist enthalpy flux along with a negative feedback as increasing wind speed can impose faster cooling of SST in turn opposing the intensification process. Prior studies indicate that about 90% of SST cooling occurs due to shear turbulent entrainment of cold deeper waters into the oceanic mixed layer region. In this context, a comprehensive analysis of ocean heat content or tropical cyclone heat potential can provide vital information on aspects related to tropical cyclone intensification.

The present study is an effort to understand the variability and short-term trends (~ 21 years) in both SST and OHC over the BoB region noted to be quite active in tropical cyclogenesis formation. Interestingly, the observed OHC trends are different as compared to the Atlantic and Pacific Ocean basins. An effort was made to correlate the tropical cyclone intensification with SST and OHC anomalies at four sub-domains that represent the northern, central, eastern and southern portions of the Bay region. This study also examined the correlation between tropical cyclone maximum sustained winds (V_{max}) obtained from Joint Typhoon Warning Centre (JTWC) against the SST data obtained from ERA-Interim at all sub-domains. The study indicates an increase in V_{max} and it correlates well with SST distribution observed over the recent years. The SST variability showed an in-phase correlation with V_{max} and that was consistent over all four sub-domains considered in this study.

Inter-annual variations in SST exhibit a pentadal oscillation warranting a separate detailed study. The observed variability along west-central and northern regions of the Bay was different as compared to the east-central and southern regions. Highest inter-annual variability is noticed during the pre- and post-monsoon seasons at northern Bay, followed by the central Bay regions. The variability is also high during pre-monsoon in the southern Bay, and in addition a contrasting difference is noticed during both pre- and post-monsoon seasons. The overall SST variability is highest during pre-monsoon season along eastern Bay that experienced a warming bias with an increase in SST by about 0.89° C as compared to the reference year 1996. In general, the warming bias observed during pre-monsoon season at northern Bay is much higher, and almost double as compared to the eastern Bay regions. For the study period 1996–2016, there is an overall increasing trend in SST, however an accelerated increase is seen from 2004 onwards having distinct increasing/decreasing cycles. This study signifies that the basin scale SST anomaly varied between 2.0 °C (maximum) to 1.7 °C (minimum) during the post-monsoon and 2.4 °C (maximum) to 1.6 °C (minimum) during the pre-monsoon seasons. The northern Bay region exhibits maximum variability attributed due to differential distribution of water mass characteristics influenced by numerous riverine inputs and complex circulation features. The study also used the reanalysis products ORAS4 and ORAS5 to determine the spatial and temporal variations in OHC anomaly.

Further, the study performed an inter-comparison on the estimated OHC between the reanalysis products ORAS4, ORAS5, and in situ RAMA buoys. The short-term (~ 21 years) increasing trends in OHC are in-phase with the SST observations, and also consistent over all the four sub-domains. The study also highlights on the necessity to perform an in-depth analysis on the role of OHC in tropical cyclone intensification. In general, it is noticed that spatial distribution of OHC anomaly during pre-monsoon is higher as compared to the post-monsoon season, unlike the distribution of SST anomaly. Interestingly, the contrasting differences in positive (negative) anomalies are noticed in the southern Bay during pre- and (post-monsoon) seasons respectively having potential implications on tropical cyclogenesis and its intensification in BoB basin. A detailed analysis was also carried out to understand the OHC variability utilizing both ORAS4 and ORAS5 data for the upper 300 m water depth during 1996–2016. Highest variability is seen at northern Bay corresponding to the buoy location almost 35% higher with reference to ORAS5. This difference reduces to 9% and 7% respectively at the central and southern Bay regions. Meridional mean time evolution of seasonal anomalies pertaining to SST and OHC distribution for the study region indicates that spatial gradients of SST anomaly during pre- and post-monsoon seasons exhibit an oscillatory cycle with episodes of alternate warm and cold bias events. In general, it is observed that warming dominates the cooling episodes for the entire BoB basin. Interestingly, the warming trend dominates basin-wide during pre-monsoon season, and since 2007, the post-monsoon seasonal OHC anomaly continued to warm over the entire Bay having a direct bearing on tropical cyclone activity and storm intensification.

Annual percentage probability of intensification for stages from depression to cyclonic storm, depression to severe cyclonic storm, and from cyclonic storm to severe cyclonic storm was 42.4%, 23.2%, and 54.7% respectively. The study clearly postulates that with an increasing trend noticed in

SST and OHC, the annual percentage probability of tropical cyclone intensification is also found higher (54.7%) for stages that transform from cyclonic storm to severe cyclonic storm. This study confirms the fact that genesis locations have a strong correlation with SST anomalies both for the pre- and post-monsoon cases, as well the spatial gradients in OHC anomalies favours the intensification. Further, the observed OHC variability has a possible tele-connection with the Oceanic Niño Index in the Pacific Ocean basin. The study highlights that positive/negative peaks in the OHC distribution has a strong in-phase relation associated with LaNiña/ElNiño events in the Pacific Ocean basin. In context to BoB, the OHC correlation magnitude increased relatively from northern to southern boundary of the Bay region. This study is believed to have potential importance in research activity related to tropical cyclone modelling.

References

Alam MM, Hossain MA, Shafee S (2003) Frequency of Bay of Bengal cyclonic storms and depressions crossing different coastal zones. Int J Climatol 23:1119–1125

Ali MM, Swain D, Kashyap T, McCreary J, Nagamani P (2013) Relationship between cyclone intensities and sea surface temperature in the Tropical Indian Ocean. IEEE Geosci Remote Sens Lett 10:841–844. https://doi.org/10.1109/LGRS.2012.2226138

Anandh TS, Das BK, Kumar B, Kuttippurath J, Chakraborty A (2018) Analyses of the oceanic heat content during 1980–2014 and satellite-era cyclones over Bay of Bengal. Int J Climatol 38:5619–5632. https://doi.org/10.1002/joc.5767

Balmaseda MA, Mogensen K, Weaver AT (2013) Evaluation of the ECMWF ocean reanalysis system ORAS4. Q J R Meteorol Soc 139(674):1132–1161

Bony S, Lau KM, Sud YC (1997) Sea surface temperature and large-scale circulation influences on tropical greenhouse effect and cloud radiative forcing. J Clim 10:2055–2077

Cane MA, Zebiak. SE, Dolan SC (1986) Experimental forecasts of El Niño. Nature 321:827–832

Cheng L, Trenberth KE, Fasullo JT, Mayer M, Balmaseda M, Zhu J (2019) Evolution of Ocean Heat Content related to ENSO. J Clim. https://doi.org/10.1175/JCLI-D-18-0607.1

Dee DP, Uppala SM, Simmons AJ, Berrisford P, Poli P, Kobayashi S, Andrae U, Balmaseda MA, Balsamo G, Bauer P, Bechtold P, Beljaars ACM, van deBerg L, Bidlot J, Bormann N, Delsol C, Dragani R, Fuentes M, Geer AJ, Haimberger L, Healy SB, Hersbach H, Holm EV, Isaksen L, Kallberg P, Kohler M, Matricardi M, McNally AP, Monge-Sanz BM, Morcrette J-J, Park B-K, Peubey C, de Rosnay P, Tavolato C, Thepaut J-N, Vitart F (2011) The ERA-Interim reanalysis: configuration and performance of the data assimilation system. Q J R Meteorol Soc 137:553–597. https://doi.org/10.1002/qj.828

Evan AT, Camargo SJ (2011) A climatology of Arabian Sea cyclonic storms. J Clim 24:140–158

Felton CS, Subrahmanyam B, Murty VSN (2013) ENSO-modulated cyclogenesis over the Bay of Bengal. J Clim 26:9806–9818

Girishkumar MS, Ravichandran M (2012) The influences of ENSO on tropical cyclone activity in the Bay of Bengal during October–December. J Geophys Res 117:C02033

Gray WM (1968) Global view of the origin of tropical disturbances and storms. Mon Weather Rev 96:669–700

Jangir B, Swain D, Ghose SK, Goyal R, Bhaskar U, T.V.S. (2019) Inter-comparison of model, satellite and in situ tropical cyclone heat potential in the North Indian Ocean. Nat Hazards. https://doi.org/10.1007/s11069-019-03756-4

Jangir B, Swain D, Ghose SK (2020) Influence of eddies and tropical cyclone heat potential on intensity changes of tropical cyclones in the North Indian Ocean. Adv Sp Res. https://doi.org/10.1016/j.asr.2020.01.011

Jin FF (1997) An equatorial recharge paradigm for ENSO. Part I: conceptual model. J Atmos Sci 54:811–829

Kossin JP, Emanuel KA, Vecchi GA (2014) The poleward migration of the location of tropical cyclone maximum intensity. Nature 509:349–352

Latif M, Grötzner A (2000) The equatorial Atlantic oscillation and its response to ENSO. Clim Dyn 16:213–218. https://doi.org/10.1007/s003820050014

Li Z, Yu W, Li T, Murty VSN, Tangang F (2013) Bimodal character of cyclone climatology in the Bay of Bengal modulated by monsoon seasonal cycle. J Clim 26:1033–1046

Li Y, Han W, Wang W, Ravichandran M, Lee T, Shinoda T (2017) Bay of Bengal salinity stratification and Indian summer monsoon intraseasonal oscillation: 2. Impact on SST and convection. J Geophys Res Oceans 122:4312–4328. https://doi.org/10.1002/2017JC012692

Magee AD, Verdon-Kidd DC (2018) On the relationship between Indian Ocean sea surface temperature variability and tropical cyclogenesis in the southwest Pacific. Int J Climatol. https://doi.org/10.1002/joc.5406

Mawren D, Reason CJC (2016) Variability of upper-ocean characteristics and tropical cyclones in the South west Indian Ocean. J Geophys Res Oceans 122:2012–2028. https://doi.org/10.1002/2016JC012028

Mayer M, Haimberger L, Balmaseda MA (2014) On the energy exchange between tropical ocean basins related to ENSO. J Clim 27:6393–6403. https://doi.org/10.1175/JCLI-D-14-00123.1

Mayer M, Balmaseda MA, Haimberger L (2018) Unprecedented 2015/2016 Indo-Pacific heat transfer speeds up tropical Pacific heat recharge. Geophys Res Lett 45:3274–3284. https://doi.org/10.1002/2018GL077106

McPhaden MJ, Meyers G, Ando K, Masumoto Y, Murty VSN, Ravichandran M, Syamsudin F, Vialard J, Yu L, Yu W (2009) RAMA: the Research Moored Array for African-Asian-Australian Monsoon Analysis and Prediction. Bull Am Meteorol Soc 90:459–480. https://doi.org/10.1175/2008BAMS2608.1

Meinen CS, McPhaden MJ (2000) Observations of warm water volume changes in the equatorial Pacific and their relationship to El Niño and La Niña. J Clim 13:3551–3559

Mogensen K, Balmaseda M, Weaver A (2012) The NEMOVAR ocean data assimilation system as implemented in the ECMWF ocean analysis for System4. In: ECMWF Technical Memorandum, 668, p 59

Mohanty UC (1994) Tropical cyclones in the Bay of Bengal and deterministic methods for prediction of their trajectories. Sadhana 19(4):567–582

Rajeevan M, McPhaden MJ (2004) Tropical Pacific upper ocean heat content variations and Indian summer monsoon rainfall. Geophys Res Lett 31:L18203. https://doi.org/10.1029/2004GL020631

Sahoo B, Bhaskaran PK (2016) Assessment on historical cyclone tracks in the Bay of Bengal, east coast of India. Int J Climatol 36(1):95–109

Sprintall J, Wijffels SE, Molcard R, Jaya I (2009) Direct estimates of the Indonesian Throughflow entering the Indian Ocean: 2004–2006. J Geophys Res 114:C07001. https://doi.org/10.1029/2008JC005257

Trenberth KE, Caron JM, Stepaniak DP, Worley S (2002) Evolution of El Niño Southern Oscillation and global atmospheric

surface temperatures. J Geophys Res 107(D8):4065. https://doi.org/10.1029/2000D000298

Vissa NK, Satyanarayana ANV, Kumar P (2013) Intensity of tropical cyclones during pre- and post-monsoon seasons in relation to accumulated tropical cyclone heat potential over Bay of Bengal. Nat Hazards 68:351–371

Wyrtki K (1985) Water displacements in the Pacific and the genesis of El Niño cycles. J Geophys Res 90:7129–7132

Yanase W, Satoh M, Taniguchi H, Fujinami H (2012) Seasonal and intraseasonal modulation of tropical cyclogenesis environment over the Bay of Bengal during the extended summer monsoon. J Clim 25:2914–2930

Yeh S-W, Cai W, Min S-K, McPhaden MJ, Dommenget D, Dewitte B, Collins M, Ashok A, An S-I, Yim B-Y, Kug J-S (2018) ENSO atmospheric teleconnections and their response to greenhouse gas forcing. Rev Geophys 56:185–206. https://doi.org/10.1002/2017RG000568

Yoo S-H, Fasullo J, Yang S, Ho C-H (2010) On the relationship between Indian Ocean sea surface temperature and the transition from El Niño to La Niña. J Geophys Res 115:D15114. https://doi.org/10.1029/2009JD012978

Zebiak S (1989) Ocean heat content variability and ENSO cycles. J Phys Oceanogr 19:475–485

Zuo H, Balmaseda MA, Mogensen K (2015) The ECMWF-My Ocean2 eddy-permitting ocean and sea-ice reanalysis ORAP5. Part I: Implementation. In: ECMWF Technical Memorandum, 736, p 44